Inorganic Chemistry
Article

Inorg. Chem. **2011**, *50*, 451–462 **451**
DOI: 10.1021/ic901834v

Cyclometalated Iridium(III) Complexes Based on Phenyl-Imidazole Ligand

Etienne Baranoff,*,† Simona Fantacci,‡,§ Filippo De Angelis,‡ Xianxi Zhang,†,# Rosario Scopelliti,† Michael Grätzel,† and Md. Khaja Nazeeruddin*,†

†*Laboratory for Photonics and Interfaces, Institute of Chemical Sciences and Engineering, School of Basic Sciences, Swiss Federal Institute of Technology, CH-1015 Lausanne, Switzerland,* ‡*Istituto CNR di Scienze e Tecnologie Molecolari, c/o Dipartimento di Chimica, Università di Perugia, via Elce di Sotto 8, I-06123 Perugia, Italy,* §*Italian Institute of Technology (IIT), Center for Biomolecular Nanotechnologies, I-73010 Arnesano, Lecce, Italy, and* #*School of Chemistry and Chemical Engineering, Liaocheng University, Liaocheng 252059, P. R. China*

Received September 17, 2009

Phenyl-imidazole-based ligands with various substitution patterns have been used as the main ligand for heteroleptic bis-cyclometalated iridium complexes. Two series of complexes have been prepared and their photophysical and electrochemical properties were studied. The phosphorescence emission maxima range from about 490 to 590 nm, that is, from greenish-blue to orange. The first series is of the form $Ir(L)_2(acac)$ (L: a phenyl-imidazole based ligand; acac: acetylacetonate). In the first complex, **1a**, L is 1,4,5-trimethyl-2-phenyl-1*H*-imidazole. Then, methyl groups are replaced with phenyl groups and chlorines are grafted on the cyclometalated phenyl ring. The second series is of the form Ir(4,5-dimethyl-1,2-diphenyl-1*H*-imidazole)$_2(L_a)$ (L_a: ancillary ligand being acetylacetonate, acac, *N*,*N*-dimethylamino-picolinate, NPic, picolinate, Pic, or 2-(diphenylphosphino)acetic acid, P). These series show that modifying the substitution pattern on the ligands can alter the photophysical and electrochemical properties of the complexes. Overall, we show that compared to complexes containing phenyl-pyridine ligands, highest occupied molecular orbitals (HOMOs) and lowest unoccupied molecular orbitals (LUMOs) are more delocalized over the entire main ligand in complexes containing phenyl-imidazole. Contrary to expectations, when chlorine atoms are used as strong acceptor substituents on the orthometalated phenyl, a red shift of the emission is observed. This behavior has been rationalized using theoretical calculations on the excited state of the chloro-substituted complex **3a** compared to the model **1a**.

Introduction

Cyclometalated iridium(III) complexes are often considered as the most promising family of triplet emitters for organic light-emitting diodes (OLEDs).[1−6] This is due to their excellent phosphorescent quantum yield and the possibility to easily tune the color of emission from deep blue to red.[7−12]

The most commonly used cyclometalated ligands are based on 2-phenyl-pyridine (ppy). Simple variation of the substitution pattern with donor and acceptor groups allows the tuning of the photophysical properties.[13−18] Another approach is to directly modify the skeleton of the main ligand

*To whom correspondence should be addressed. E-mail: etienne.baranoff@epfl.ch (E.B.); mdkhaja.nazeeruddin@epfl.ch (M.K.N.).

(1) Tanaka, D.; Sasabe, H.; Li, Y.-J.; Su, S.-J.; Takeda, T.; Kido, J. *Jpn. J. Appl. Phys., Part 2* **2007**, *46*, L10.
(2) Gustafsson, G.; Cao, Y.; Treacy, G. M.; Klavetter, F.; Colaneri, N.; Heeger, A. J. *Nature* **1992**, *357*, 477.
(3) Baldo, M. A.; O'Brien, D. F.; You, Y.; Shoustikov, A.; Sibley, S.; Thompson, M. E.; Forrest, S. R. *Nature* **1998**, *395*, 151.
(4) *Highly Efficient OLEDs with Phosphorescent Materials*; Yersin, H., Ed.; Wiley-VCH: Berlin, 2007.
(5) Yersin, H. *Top. Curr. Chem.* **2004**, *241*, 1.
(6) Evans, R. C.; Douglas, P.; Winscom, C. J. *Coord. Chem. Rev.* **2006**, *250*, 2093.
(7) Baranoff, E.; Yum, J.-H.; Graetzel, M.; Nazeeruddin, M. K. *J. Organomet. Chem.* **2009**, *694*, 2661.
(8) Flamigni, L.; Barbieri, A.; Sabatini, C.; Ventura, B.; Barigelletti, F. *Top. Curr. Chem.* **2007**, *281*, 143.
(9) Lowry, M. S.; Bernhard, S. *Chem.—Eur. J.* **2006**, *12*, 7970.
(10) Chou, P.-T.; Chi, Y. *Chem.—Eur. J.* **2007**, *13*, 380.
(11) Wong, W.-Y.; Ho, C.-L. *Coord. Chem. Rev.* **2009**, *253*, 1709.
(12) You, Y.; Park, S. Y. *Dalton Trans.* **2009**, 1267.
(13) Dedeian, K.; Djurovich, P. I.; Garces, F. O.; Carlson, G.; Watts, R. J. *Inorg. Chem.* **1991**, *30*, 1687.
(14) Tamayo, A. B.; Alleyne, B. D.; Djurovich, P. I.; Lamansky, S.; Tsyba, I.; Ho, N. N.; Bau, R.; Thompson, M. E. *J. Am. Chem. Soc.* **2003**, *125*, 7377.
(15) Baranoff, E.; Suarez, S.; Bugnon, P.; Bolink, H. J.; Klein, C.; Scopelliti, R.; Zuppiroli, L.; Grätzel, M.; Nazeeruddin, M. K. *ChemSusChem* **2009**, *2*, 305.
(16) Zhou, G.; Ho, C.-L.; Wong, W.-Y.; Wang, Q.; Ma, D.; Wang, L.; Lin, Z.; Marder, T. B.; Beeby, A. *Adv. Funct. Mater.* **2008**, *18*, 499.
(17) Takizawa, S.-Y.; Echizen, H.; Nishida, J.-I.; Tsuzuki, T.; Tokito, S.; Yamashita, Y. *Chem. Lett.* **2006**, *35*, 748.
(18) Avilov, I.; Minoofar, P.; Cornil, J.; De Cola, L. *J. Am. Chem. Soc.* **2007**, *129*, 8247.

Published on Web 12/14/2010

Scheme 1. Molecular Structures of Complexes

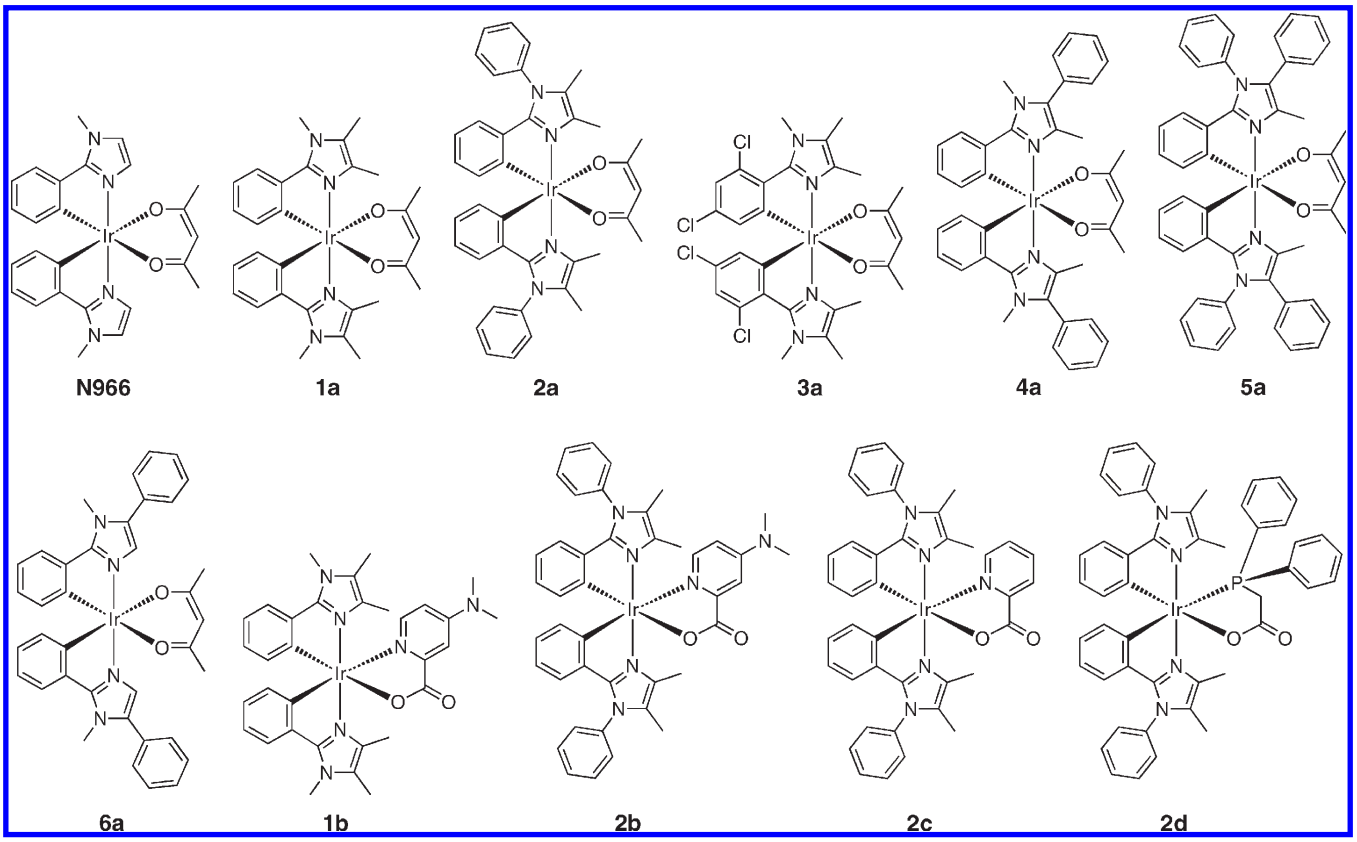

by using various heterocyclic rings instead of pyridine.[19−25] A commonly used heterocyclic ring for undertaking such tuning is 2-phenyl-benzimidazole.[26−32] Surprisingly, it appears that cyclometalated iridium complexes using a 2-phenyl-imidazole ligand without the fused benzene ring (i.e., not based on benzo-[*d*]imidazole motif) are hardly reported in the literature.[33−35]

Recently, we reported an iridium complex without a fused benzene ring, acetylacetonato bis(1-methyl-2-phenylimidazole) iridium(III), hereafter labeled **N966**.[36,37] The **N966** complex exhibits unique photophysical behavior as the lowest unoccupied molecular orbitals (LUMOs) of the main ligand and of the ancillary ligand are almost degenerate, which leads to broad photo- and electro-phosphorescence. This makes this dopant suitable for white organic light-emitting diode (WOLED) based on a single emitting center. To gain insight into this class of molecules, we prepared complexes related to **N966**, with various substitution patterns. In this manuscript, we report our initial results on this family of iridium complexes with a focus on heteroleptic complexes (Scheme 1, Chart 1). It includes synthesis and electrochemical and photophysical characterizations. Finally, we focus on the unexpected red-shifting effect of the chloro substitution with theoretical calculations to rationalize this counterintuitive experimental result.

Experimental Procedures

Materials and General Considerations. The solvents (puriss. grade) and starting materials were purchased from Fluka and

(19) Lamansky, S.; Djurovich, P.; Murphy, D.; Abdel-Razzaq, F.; Lee, H.-E.; Adachi, C.; Burrows, P. E.; Forrest, S. R.; Thompson, M. E. *J. Am. Chem. Soc.* **2001**, *123*, 4304.
(20) Lamansky, S.; Djurovich, P.; Murphy, D.; Abdel-Razzaq, F.; Kwong, R..; Tsyba, I.; Bortz, M.; Mui, B.; Bau, R.; Thompson, M. E. *Inorg. Chem.* **2001**, *40*, 1704.
(21) Tsuboyama, A.; Iwawaki, H.; Furugori, M.; Mukaide, T.; Kamatani, J.; Igawa, S.; Moriyama, T.; Miura, S.; Takiguchi, T.; Okada, S.; Hoshino, M.; Ueno, K. *J. Am. Chem. Soc.* **2003**, *125*, 12971.
(22) Song, Y.-H.; Chiu, Y.-C.; Chi, Y.; Cheng, Y.-M.; Lai, C.-H.; Chou, P.-T.; Wong, K.-T.; Tsai, M.-H.; Wu, C.-C. *Chem.—Eur. J.* **2008**, *14*, 5423.
(23) Zhou, G.; Wong, W.-Y.; Yao, B.; Xie, Z.; Wang, L. *Angew. Chem., Int. Ed.* **2007**, *46*, 1149.
(24) Ho, C.-L.; Wong, W.-Y.; Gao, Z.-Q.; Chen, C.-H.; Cheah, K.-W.; Yao, B.; Xie, Z.; Wang, Q.; Ma, D.; Wang, L.; Yu, X.-M.; Kwok, H.-S.; Lin, Z. *Adv. Funct. Mater.* **2008**, *18*, 319.
(25) Sajoto, T.; Djurovich, P. I.; Tamayo, A.; Yousufuddin, M.; Bau, R.; Thompson, M. E. *Inorg. Chem.* **2005**, *44*, 7992.
(26) Chen, L.; Yang, C.; Qin, J.; Gao, J; Ma, D. *Inorg. Chim. Acta* **2006**, *359*, 4207.
(27) Huang, W.-S.; Lin, J. T.; Chien, C.-H.; Tao, Y.-T.; Sun, S.-S.; Wen, Y.-S. *Chem. Mater.* **2004**, *16*, 2480.
(28) Velusamy, M.; Thomas, K. R. J.; Chen, C.-H.; Lin, J. T.; Wen, Y. S.; Hsieh, W.-T.; Lai, C.-H.; Chou, P.-T. *Dalton Trans.* **2007**, *28*, 3025.
(29) Wei, X.; Peng, J.; Cheng, J.; Xie, M.; Lu, Z.; Li, C.; Cao, Y. *Adv. Funct. Mater.* **2007**, *17*, 3319.
(30) Ding, J.; Gao, J.; Cheng, Y.; Xie, Z.; Wang, L.; Ma, D.; Jing, X.; Wang, F. *Adv. Funct. Mater.* **2006**, *16*, 575.
(31) Obara, S.; Itabashi, M.; Okuda, F.; Tamaki, S.; Tanabe, Y.; Ishii, Y.; Nozaki, K.; Haga, M. *Inorg. Chem.* **2006**, *45*, 8907.
(32) Yukata, T.; Obara, S.; Ogawa, S.; Nozaki, K.; Ikeda, N.; Ohno, T.; Ishii, Y.; Sakai, K.; Haga, M. *Inorg. Chem.* **2005**, *44*, 4737.
(33) Treboux, G.; Mizukami, J.; Yabe, M.; Nakamura, S. *J. Photopol. Sci. Technol.* **2008**, *21*, 347.
(34) Ashizawa, M.; Yang, L.; Kobayashi, K.; Sato, H.; Yamagishi, A.; Okuda, F.; Harada, T.; Kuroda, R.; Haga, M. *Dalton Trans.* **2009**, *10*, 1700.
(35) Giebink, N. C.; D'Andrade, B. W.; Weaver, M. S.; Mackenzie, P. B.; Brown, J. J.; Thompson, M. E.; Forrest, S. R. *J. Appl. Phys.* **2008**, *103*, 044509.
(36) Bolink, H. J.; De Angelis, F.; Baranoff, E.; Klein, C.; Fantacci, S.; Coronado, E.; Sessolo, M.; Kalyanasundaram, K.; Grätzel, M.; Nazeeruddin, M. K. *Chem. Commun.* **2009**, 4672.
(37) Nazeeruddin, M. K.; Klein, C.; Graetzel, M. PCT Int. Appl. 2008, WO 2008043815.

Chart 1. Substitution Patterns for Ligands, Dimers, and Complexes

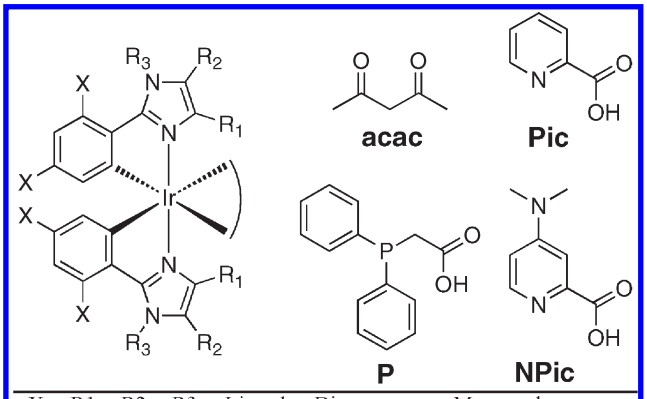

X	R1	R2	R3	Ligand	Dimer	Mononuclear			
						acac	pic	Npic	P
-H	-Me	-Me	-Me	L1	**1**	**1a**		**1b**	
-H	-Me	-Me	-Ph	L2	**2**	**2a**	**2c**	**2b**	**2d**
-Cl	-Me	-Me	-Me	L3	**3**	**3a**			
-H	-Me	-Ph	-Me	L4	**4**	**4a**			
-H	-Me	-Ph	-Ph	L5	**5**	**5a**			
-H	-H	-Ph	-Me	L6	**6**	**6a**			
-H	-H	-H	-Me			**N966**			

Sigma-Aldrich and used as received. Hydrated iridium trichloride was used as received from Heraeus. UV−visible spectra were recorded in a 1 cm path length quartz cell on a Cary 5 spectrophotometer. Emission spectra were recorded on a Fluorolog 3-22 using a 90° optical geometry. The emission spectra were photometrically corrected using a NBS calibrated 200 W tungsten lamp as a reference source. Lifetime of excited state measurements using a FL-1061PC TCSPC and 371 and 406 nm Nanoled as the excitation source. Voltammetric measurements employed a PC controlled AutoLab PSTAT10 electrochemical workstation. Cyclic voltammograms (CV) were obtained at a scan rate of 100 mV/s using 0.1 M $TBAPF_6$ as supporting electrolyte in dimethylformamide (DMF). Glassy carbon, sputtered platinum, and platinum wire were employed as working, counter, and reference electrodes, respectively. At the end of each measurement, the ferrocenium/ferrocene (Fc^+/Fc) potential was measured and used as an internal reference. NMR spectra were measured with a Bruker AV-400 spectrometer, and the reported chemical shifts were referenced to tetramethylsilane $SiMe_4$. The data collections from X-ray crystallography were performed at low temperature using Mo K_α radiation. A Bruker APEX II CCD, having kappa geometry, was employed for **1a** and **2b**, while **4a** was measured on a marμX system. The data of **1a** and **2b** were reduced by means of EvalCCD[38] and then corrected for absorption,[39] whereas *automar*[40] was used for the treatment of the data belonging to compound **4a**. The solutions and refinements were performed by SHELX.[41] The structures were refined using full-matrix least-squares based on F^2 with all nonhydrogen atoms anisotropically defined. Hydrogen atoms were placed in calculated positions by means of the "riding" model.

The geometries of the investigated complexes were optimized under C_2 symmetry constraints using the BP86 exchange-correlation functional,[42,43] together with a TZP (DZP) basis set for Ir (N, C, H), including scalar-relativistic corrections as implemented in the ADF program.[44] At the optimized geometries, we performed ground and excited state DFT/TDDFT calculations at the B3LYP/LANL2DZ level of theory[45,46] in CH_2Cl_2 solution by means of the PCM solvation model,[47] as implemented in the Gaussian 03 program package.[48] The nonequilibrium[49] implementation of the PCM algorithm was used for TDDFT calculations. Both singlet−singlet and singlet−triplet TDDFT excitations have been computed.

Zinc powder was activated as follows: the zinc powder is stirred in 1 N HCl solution for 20 min. The powder is filtered and washed successively with water, acetone, and Et_2O. The powder is then dried in an oven at 80 °C for 2 h, cooled down, and used as is.

L1, 1,4,5-Trimethyl-2-phenylimidazole. Benzaldehyde (5.3 g, 0.049 mol), 40% aq. methylamine (3.90 g, 0.049 mol), and 2,3-butanedione monoxime (4.95 g, 0.049 mol) were added to glacial acetic acid (60 mL). After being refluxed for 2 h, the orange solution was cooled, and zinc (15 g, activated granules) was added. The resulting mixture was refluxed for 1 h and then kept overnight at room temperature. The suspension was filtered off and washed with water. Treatment of the filtrate with ammonium hydroxide resulted in the separation of a yellow oil, which was extracted with toluene (3 × 100 mL). The combined organic extracts were dried with anhydrous magnesium sulfate, filtered, and then concentrated under a vacuum to give a brown-orange viscous oil, which was purified by column chromatography (SiO_2, CH_2Cl_2/MeOH 5%) to give a viscous yellow orange oil which crystallized on standing (1.8 g, y: 20%). ^{1}H NMR ($CDCl_3$, 400 MHz): δ 7.59−7.54 (m, 2H); 7.45−7.29 (m, 3H); 3.54 (s, 3H); 2.22 (s, 3H); 2.19 (s, 3H). ^{13}C NMR ($CDCl_3$, 100 MHz): δ 146.02, 133.20, 131.37, 128.90, 128.64, 128.43, 124.36, 32.12, 12.84, 9.40. TOF HRMS ES: MH^+ m/z: calc. 187.1235 found: 187.1238.

L2, 4,5-Dimethyl-1,2-diphenylimidazole. Benzaldehyde (5.3 g, 0.049 mol), aniline (4.65 g, 0.05 mol), and 2,3-butanedione monoxime (4.95 g, 0.049 mol) were added to glacial acetic acid (60 mL). After being refluxed for 2 h, the orange solution was cooled, and zinc (20 g, activated granules) was added. The resulting mixture was refluxed for 3 h and then kept overnight at room temperature. The suspension was filtered off and washed with water. Treatment of the filtrate with ammonium hydroxide resulted in the separation of a yellow oil, which was extracted with toluene (3 × 100 mL). The combined organic extracts were dried with anhydrous magnesium sulfate, filtered, and then concentrated under a vacuum to give a brown-orange viscous oil, which was purified with column chromatography (SiO_2, EtOAc/Et_2O 50%) to give a beige solid (4.9 g, y: 40%). ^{1}H NMR ($CDCl_3$, 400 MHz): δ 7.46−7.40 (m, 3H); 7.33−7.28 (m, 2H); 7.21−13 (m, 5H); 2.19 (s, 3H); 2.01 (s, 3H). ^{13}C NMR ($CDCl_3$, 100 MHz): δ 145.28, 137.81, 133.33, 130.39, 129.77, 128.81, 128.49, 128.29, 128.15, 128.13, 125.64, 12.50, 9.74. TOF HRMS ES: MH^+ m/z: calc. 249.1392 found: 249.1400.

(38) Duisenberg, A. J. M.; Kroon-Batenburg, L. M. J.; Schreurs, A. M. M. *J. Appl. Crystallogr.* **2003**, *36*, 220.
(39) Blessing, R. H. *Acta Crystallogr., Sect. A* **1995**, *51*, 33.
(40) *automar*, release 2.7.1; Klein, C.; Bartels, K.; Marresearch GmbH: Norderstedt, Germany, 2010.
(41) *SHELX*; Sheldrick, G. M. *Acta Crystallogr., Sect. A* **2008**, *64*, 112.
(42) Becke, A. D. *Phys. Rev. A* **1988**, *38*, 3098.
(43) Perdew, J. P. *Phys. Rev. B* **1986**, *33*, 8822.
(44) te Velde, G.; Bickelhaupt, M. F.; Baerends, E. J.; Fonseca-Guerra, C.; van Gisbergen, S. J. A.; Snijders, J. G.; Ziegler, T. *J. Comput. Chem.* **2001**, *22*, 931.
(45) Becke, A. D. J. *Chem. Phys.* **1993**, *98*, 5648.
(46) Hay, P. J.; Wadt, W. R. *J. Chem. Phys.* **1985**, *82*, 270.
(47) Miertus, S.; Scrocco, S.; Tomasi, J. *Chem. Phys.* **1981**, *55*, 117.
(48) Frisch, M. J.; Trucks, G. W.; Schlegel, H. B.; Scuseria, G. E.; Robb, M. A.; Cheeseman, J. R.; Montgomery, J. A.; , Jr., Vreven, T.; Kudin, K. N.; Burant, J. C.; Millam, J. M.; Iyengar, S. S.; Tomasi, J.; Barone, V.; Mennucci, B.; Cossi, M.; Scalmani, G.; Rega, N.; Petersson, G. A.; Nakatsuji, H.; Hada, M.; Ehara, M.; Toyota, K.; Fukuda, R.; Hasegawa, J.; Ishida, M.; Nakajima, T.; Honda, Y.; Kitao, O.; Nakai, H.; Klene, M.; Li, X.; Knox, J. E.; Hratchian, H. P.; Cross, J. B.; Adamo, C.; Jaramillo, J.; Gomperts, R.; Stratmann, R. E.; Yazyev, O.; Austin, A. J.; Cammi, R.; Pomelli, C.; Ochterski, J. W.; Ayala, P. Y.; Morokuma, K.; Voth, G. A.; Salvador, P.; Dannenberg, J. J.; Zakrzewski, V. G.; Dapprich, S.; Daniels, A. D.; Strain, M. C.; Farkas, O.; Malick, D. K.; Rabuck, A. D.; Raghavachari, K.; Foresman, J. B.; Ortiz, J. V.; Cui, Q.; Baboul, A. G.; S. Clifford, J. *Gaussian 03*, Revision B05; Gaussian, Inc.: Pittsburgh, PA, 2003.
(49) Cossi, M.; Barone, V. J. *Chem. Phys.* **2001**, *115*, 4708.

L3, 2-(2,4-Dichlorophenyl)-1,4,5-trimethylimidazole. 2,4-Dichloro-benzaldehyde (2.15 g, 0.012 mol), 40% aq. methylamine (0.96 g, 0.012 mol), and 2,3-butanedione monoxime (1.24 g, 0.012 mol) were added to glacial acetic acid (20 mL). After being refluxed for 2.5 h, the orange solution was cooled, and zinc (12 g, activated granules) was added. The resulting mixture was refluxed for 3 h and then kept overnight at room temperature. The suspension was filtered off and washed with water. Treatment of the filtrate with ammonium hydroxide resulted in the separation of a yellow oil, which was extracted with toluene (3 × 100 mL). The combined organic extracts were dried with anhydrous magnesium sulfate, filtered, and then concentrated under a vacuum to give a brown-orange viscous oil, which was purified with column chromatography (SiO_2, CH_2Cl_2/MeOH 0−10%) to give a beige solid (1.5 g, y: 48%). ^{1}H NMR ($CDCl_3$, 400 MHz): δ 7.68 (d, 1H, J = 8.4 Hz); 7.66 (d, 1H, J = 2.0 Hz); 7.51 (dd, 1H, J = 8.4 Hz, J = 2 Hz); 3.48 (s, 3H); 2.36 (s, 3H); 2.34 (s, 3H). ^{13}C NMR ($CDCl_3$, 100 MHz): δ 152.45, 137.59, 136.27, 134.73, 130.29, 128.09, 126. 68, 123.03, 121.52, 31.73, 9.28, 7.52. TOF HRMS ES: MH^+ m/z: calc. 255.0456 found: 255.0452.

L4, 1,4-Dimethyl-2,5-diphenylimidazole. Benzaldehyde (4.08 g, 0.038 mol), 40% aq. methylamine (3.00 g, 0.038 mol), and 1-phenyl-1,2-propanedione-2-oxime (6.27 g, 0.038 mol) were added to glacial acetic acid (70 mL). After being refluxed for 5 h, the yellow solution was cooled, and zinc (20 g, activated granules) was added. The resulting mixture was refluxed for 2 h and then kept overnight at room temperature. The suspension was filtered off and washed with water. After treatment of the filtrate with ammonium hydroxide, the filtrate was extracted with CH_2Cl_2 (3 × 100 mL). The combined organic extracts were washed with water and brine, dried with anhydrous magnesium sulfate, filtered, and then concentrated under a vacuum to give a viscous oil, which was purified with column chromatography (SiO_2, EtOAc/Et_2O 10/90 to 100/0) to give a viscous colorless oil which crystallized upon addition of a few drops of toluene. After drying, the compound is obtained as a white solid (2.6 g, y: 27%). No isomer is detected in the crude.[50] ^{1}H NMR ($CDCl_3$, 400 MHz): δ 7.69−7.65 (m, 2H); 7.50−7.34 (m, 8H); 3.54 (s, 3H); 2.29 (s, 3H). ^{13}C NMR ($CDCl_3$, 100 MHz): δ 147.59, 135.36, 131.23, 130.92, 130.82, 130.24, 129.04, 128.86, 128.72, 127.91, 33.88, 13.64. TOF HRMS ES: MH^+ m/z: calc. 249.1392 found: 249.1400.

L5, 4-Methyl-1,2,5-triphenylimidazole. Benzaldehyde (4.07 g, 0.038 mol), aniline (3.57 g, 0.038 mol), and 1-phenyl-1,2-propanedione-2-oxime (6.24 g, 0.038 mol) were added to glacial acetic acid (60 mL). After being refluxed for 3 h, the dark orange solution was cooled, and zinc (20 g, activated 10 μm dust) was added. The resulting mixture was refluxed for 1.5 h and then kept overnight at room temperature. The suspension was filtered off and washed with water. After treatment of the filtrate with ammonium hydroxide, the filtrate was extracted with CH_2Cl_2 (3 × 100 mL). The combined organic extracts were washed with water and brine, dried with anhydrous magnesium sulfate, filtered, and then concentrated under a vacuum until a white precipitate appeared. EtOH was added and the white precipitate was filtered off. Filtrate was evaporated, dissolved in a minimum of CH_2Cl_2, and Et_2O was added. The slightly beige precipitate was filtered off. After drying, the compound was obtained as beige a solid (10.48 g, y: 88%). ^{1}H NMR ($CDCl_3$, 400 MHz): δ 7.30−7.14 (m, 11H); 7.08−7.01 (m, 4H); 2.23 (s, 3H). ^{13}C NMR ($CDCl_3$, 100 MHz): δ 144.44, 135.63, 131.40, 130.53, 130.37, 129.91, 129.64, 129.44, 128.94, 128.88, 128.77, 128.69, 128.19, 127.85, 120.08, 11.74. TOF HRMS ES: MH^+ m/z: calc. 311.1548 found: 311.1544.

(50) Lantos, I.; Zhang, W.-Y.; Shui, X.; Eggleston, D. S. *J. Org. Chem.* **1993**, *58*, 7092.

L6, 1-Methyl-2,5-diphenylimidazole. Benzaldehyde (4.6 g, 0.043 mol), 40% aq. methylamine (3.37 g, 0.043 mol), and 2-isonitrosoacetophenone (6.44 g, 0.043 mol) were added to glacial acetic acid (60 mL). After being refluxed for 3 h, the dark orange solution was cooled, and zinc (20 g, activated 10 μm dust) was added. The resulting mixture was refluxed for 1.5 h and then kept overnight at room temperature. The suspension was filtered off and washed with water. After treatment of the filtrate with ammonium hydroxide, the filtrate was extracted with toluene (3 × 100 mL). The combined organic extracts were washed with water and brine, dried with anhydrous magnesium sulfate, filtered, and then adsorbed on silica gel. Chromatography column purification was performed using silica and CH_2Cl_2/MeOH 1% as the eluent to yield **L6** as a white solid (4.11 g, y: 40%). ^{1}H NMR ($CDCl_3$, 400 MHz): δ 7.69 (m, 2H); 7.51−7.32 (m, 8H); 7.19 (s, 1H); 3.67 (s, 3H). ^{13}C NMR ($CDCl_3$, 100 MHz): δ 149.64, 135.67, 131.18, 130.52, 129.05, 129.02, 128.93, 128.90, 128.80, 128.13, 127.80, 34.02. TOF HRMS ES: MH^+ m/z: calc. 235.1235 found: 235.1225.

General Method for Synthesis of Chloro-Bridged Dimers. $IrCl_3 \cdot xH_2O$ was dissolved in a mixture of 2-ethoxyethanol/H_2O 3:1 (about 20 mL for 100 mg) by heating under argon around 60 °C for 30 min. The ligand in 2-ethoxyethanol (2.5 eq., 5−15 mL) was added and the solution was heated at 120 °C overnight. After cooling to RT, water was added and the precipitate was filtered, washed with water and ether and dried, and used without further purification.

1a: The dimeric iridium(III) complex **1** (94 mg; 0.078 mM) was dissolved in 100 mL of dichloromethane solvent under argon. To this solution was added acetylacetone ligand (30 mg, 0.30 mM) and tetrabutylammonium hydroxide (159 mg, 0.199 mM). The reaction mixture was refluxed under argon overnight. After being cooled to RT, the solvents evaporated to dryness. The crude obtained was purified with column chromatography (SiO_2, CH_2Cl_2) followed by further purification on SiO_2 TLC, CH_2Cl_2/MeOH 3%. The major yellow band was collected to afford **1a** as a pale yellow solid (18 mg, 17%). ^{1}H NMR ($CDCl_3$, 400 MHz): δ 7.34 (dd, 2H, J = 1.2 Hz, J = 7.6 Hz); 6.69 (dt, 2H, J = 1.2 Hz, J = 7.6 Hz); 6.56 (dt, 2H, J = 1.2 Hz, J = 7.6 Hz); 6.39 (dd, 2H, J = 1.2 Hz, J = 7.6 Hz); 5.19 (s, 1H); 3.90 (s, 6H); 2.24 (s, 6H); 2.14 (s, 6H); 1.67 (s, 6H). TOF MS ES: MH^+ m/z: calc. 662.2233 found: 662.2218 Anal. Calcd. for $C_{29}H_{33}IrN_4O_2 \cdot CH_2Cl_2$: C, 48.25; H, 4.72; N, 7.50. Found: C, 48.18; H, 4.52; N, 7.19.

1b: The dimeric iridium(III) complex **1** (102 mg; 0.085 mM) was dissolved in 100 mL of dichloromethane solvent under argon. To this solution was added methyl 4-(dimethylamino)-pyridine-2-carboxylate ligand (35 mg, 0.194 mM) and tetrabutylammonium hydroxide (270 mg, 0.337 mM). The reaction mixture was refluxed under argon for 9 h. After being cooled to RT, water was added and the mixture was extracted with dichloromethane, and the organic layer was washed with water and brine, dried over $MgSO_4$ and the solvents were evaporated to dryness. The crude obtained was purified with column chromatography (SiO_2, CH_2Cl_2/MeOH 5%) followed by further purification on SiO_2 TLC, CH_2Cl_2/MeOH 7%. The major yellow band was collected to afford **1b** as a yellow solid (23 mg, 19%). ^{1}H NMR ($CDCl_3$, 400 MHz): δ 7.50 (d, 1H, J = 2.8 Hz); 7.43−7.37 (m, 2H); 7.24 (d, 1H, J = 3.2 Hz); 6.80 (dt, 1H, J = 1.6 Hz, J = 6.8 Hz); 6.74 (dt, 1H, J = 1.6 Hz, J = 8.0 Hz); 6.70−6.60 (m, 3H); 6.36−6.30 (m, 2H); 3.90 (s, 3H); 3.86 (s, 3H); 3.01 (s, 6H); 2.15 (s, 3H); 2.12 (s, 3H); 1.53 (s, 3H); 1.39 (s, 3H). TOF MS ES: MH^+ m/z: calc. 728.2451 found: 728.2449 Anal. Calcd. for $C_{32}H_{35}IrN_6O_2$: C, 52.80; H, 4.85; N, 11.55. Found: C, 52.64; H, 4.52; N, 11.47.

2a: The dimeric iridium(III) complex **2** (117 mg; 0.081 mM) was dissolved in 100 mL of dichloromethane solvent under argon. To this solution was added acetylacetone ligand (30 mg, 0.30 mM) and tetrabutylammonium hydroxide (220 mg, 0.275 mM).

The reaction mixture was refluxed under argon overnight. After being cooled to RT, the solvents were evaporated to dryness. Ethanol (2 mL) was used to dissolve the crude product obtained and water (50 mL) was added. The precipitate was filtrated and washed with water and Et_2O. The solid obtained was dissolved in MeOH and purified on Sephadex LH-20 using MeOH as a mobile phase to afford **2a** as a brownish solid (32 mg, 38%). ^{1}H NMR ($CDCl_3$, 400 MHz): δ 7.62−7.52 (m, 6H); 7.47−7.44 (m, 2H); 7.38−7.35 (m, 2H); 6.55 (dt, 2H, J = 1.2 Hz, J = 7.6 Hz); 6.50 (dd, 2H, J = 1.2 Hz, J = 7.6 Hz); 6.36 (dt, 2H, J = 1.6 Hz, J = 7.2 Hz); 6.08 (dd, 2H, J = 1.2 Hz, J = 8.0 Hz); 5.30 (s, 1H); 2.22 (s, 6H); 2.02 (s, 6H); 1.79 (s, 6H). TOF MS ES: MH^+ m/z: calc. 786.2546 found: 786.2548 Anal. Calcd. for $C_{39}H_{37}IrN_4O_2$: C, 59.60; H, 4.75; N, 7.13. Found: C, 59.48; H, 4.53; N, 6.89.

2b: The dimeric iridium(III) complex **2** (206 mg; 0.142 mM) was dissolved in 200 mL of dichloromethane solvent under argon. To this solution was added methyl 4-(dimethylamino)pyridine-2-carboxylate ligand (92 mg, 0.51 mM) and tetrabutyl-ammonium hydroxide (450 mg, 0.562 mM). The reaction mixture was refluxed under argon overnight. After being cooled to RT, the solvents were evaporated to dryness. MeOH (2 mL) was used to dissolve the crude product obtained and water (50 mL) was added. The precipitate was filtrated and washed with water and Et_2O. The solid obtained was dissolved in MeOH and purified on Sephadex-LH20 using MeOH as a mobile phase to afford **2b** as an orange solid (47 mg, 29%). ^{1}H NMR ($CDCl_3$, 400 MHz): δ 7.65−7.47 (m, 8H); 7.38−7.31 (m, 4H); 6.73 (d, 1H, J = 7.2 Hz); 6.60 (m, 2H); 6.48−6.38 (m, 4H); 6.17 (d, 1H, J = 7.6 Hz); 6.10 (d, 1H, J = 7.6 Hz); 3.06 (s, 6H); 2.20 (s, 3H); 1.93 (s, 3H); 1.89 (s, 3H); 1.46 (s, 3H). TOF MS ES: MH^+ m/z: calc. 852.2764 found: 852.2748 Anal. Calcd. for $C_{42}H_{39}IrN_6O_2\cdot$ MeOH: C, 59.21; H, 4.61; N, 9.86. Found: C, 58.98; H, 4.56; N, 9.77.

2c: The dimeric iridium(III) complex **2** (124 mg; 0.086 mM) was dissolved in 100 mL of dichloromethane solvent under argon. To this solution was added 2-picolinic acid ligand (41 mg, 0.33 mM) and tetrabutylammonium hydroxide (522 mg, 0.652 mM). The reaction mixture was refluxed under argon for 10 h. After being cooled to RT, the solvents were evaporated to dryness. Ethanol (2 mL) was used to dissolve the crude product obtained and water (50 mL) was added. The precipitate was filtrated and washed with water and Et_2O. The solid obtained was dissolved in MeOH and purified on Sephadex-LH-20 using MeOH as a mobile phase to afford **2c** as a brownish solid (49 mg, 50%). ^{1}H NMR ($CDCl_3$, 400 MHz): δ 8.28 (d, 1H, J = 7.6 Hz); 7.86 (dt, 1H, J = 1.6 Hz, J = 7.6 Hz); 7.80 (d, 1H, J = 7.6 Hz); 7.65−7.45 (m, 8H); 7.37−7.27 (m, 3H); 6.73 (d, 1H, J = 7.2 Hz); 6.63 (dq, 2H, J = 1.2 Hz, J = 7.6 Hz); 6.50 (t, 1H, J = 8.0 Hz); 6.41 (t, 2H, J = 7.6 Hz); 6.17 (d, 1H, J = 7.6 Hz); 6.13 (d, 1H, J = 7.6 Hz); 2.19 (s, 3H); 1.94 (s, 3H); 1.88 (s, 3H); 1.33 (s, 3H). TOF MS ES: MH^+ m/z: calc. 809.2343 found: 809.2334 Anal. Calcd. for $C_{40}H_{34}IrN_5O_2\cdot CH_2Cl_2$: C, 55.09; H, 4.06; N, 7.83. Found: C, 55.08; H, 4.12; N, 7.69.

2d: The dimeric iridium(III) complex **2** (76 mg; 0.052 mM) was dissolved in 120 mL of dichloromethane solvent under argon. To this solution was added 2-(diphenylphosphino)-ethanoic acid ligand (45 mg, 0.184 mM) and tetrabutylammonium hydroxide (300 mg, 0.375 mM). The reaction mixture was refluxed under argon overnight. After being cooled to RT, the solvents were evaporated to dryness. The crude obtained was dissolved in a minimum of methanol and water was added. The precipitate was filtrated and washed with water and Et_2O. The solid was purified with column chromatography (SiO_2, CH_2Cl_2/MeOH 0−5%) followed by further purification on SiO_2 TLC, CH_2Cl_2/MeOH 5%. The major band was collected to afford **2d** as a colorless solid (16 mg, 25%). ^{1}H NMR ($CDCl_3$, 400 MHz): δ 7.69−7.46 (m, 7H); 7.40 (m, 1H); 7.32−7.22 (m, 4H); 7.19−7.07 (m, 8H); 6.93 (d, 1H, J = 7.2 Hz); 6.70 (td, 1H, J = 1.2 Hz, J = 7.4 Hz); 6.63 (tt, 1H, J = 1.4 Hz, J = 7.4 Hz); 6.57 (t, 1H, J = 7.4 Hz); 6.45 (td, 1H, J = 1.2 Hz, J = 7.2 Hz); 6.34 (t, 1H, J = 7.2 Hz); 6.21 (dd, 1H, J = 1.4 Hz, J = 8.0 Hz); 6.09 (d, 1H, J = 8.0 Hz); 4.06 (m, 1H); 3.54 (m, 1H); 1.91 (s, 3H); 1.86 (s, 3H); 1.73 (s, 3H); 1.63 (s, 3H). TOF MS ES: MH^+ m/z: calc. 930.2675 found: 930.2648 Anal. Calcd. for $C_{48}H_{42}IrN_4O_2P\cdot CH_3OH$: C, 61.17; H, 4.82; N, 5.82. Found: C, 61.02; H, 4.26; N, 5.67.

3a: The dimeric iridium(III) complex **3** (180 mg; 0.122 mM) was dissolved in 200 mL of dichloromethane solvent under argon. To this solution was added acetylacetone ligand (40 mg, 0.40 mM) and tetrabutylammonium hydroxide (359 mg, 0.448 mM). The reaction mixture was refluxed under argon overnight. After being cooled to RT, the solvents were evaporated to dryness. The crude obtained was purified with column chromatography (SiO_2, CH_2Cl_2) followed by further purification on SiO_2 TLC, CH_2Cl_2/petroleum ether 40%. The major yellow band was collected to afford **3a** as a yellow solid (22 mg, 22%). ^{1}H NMR ($CDCl_3$, 400 MHz): δ 6.81 (d, 2H, J = 2.0 Hz); 5.93 (d, 2H, J = 2.0 Hz); 5.23 (s, 1H); 3.90 (s, 6H); 2.27 (s, 6H); 2.08 (s, 6H); 1.71 (s, 6H). TOF MS ES: MH^+ m/z: calc. 798.0674 found: 798.0666 Anal. Calcd. for $C_{29}H_{29}Cl_4IrN_4O_2$: C, 43.56; H, 3.66; N, 7.01. Found: C, 43.44; H, 3.53; N, 6.81.

4a: The dimeric iridium(III) complex **4** (60 mg; 0.042 mM) was dissolved in 80 mL of dichloromethane under argon. To this solution was added acetylacetone (20 mg, 0.20 mM) and tetrabutylammonium hydroxide (186 mg, 0.248 mM). The reaction mixture was refluxed under argon overnight. After being cooled to RT, the solvents were evaporated to dryness. The crude obtained was purified with a short column chromatography (SiO_2, CH_2Cl_2). The major yellow band was collected to afford **4a** as a yellow solid (52 mg, 60%). ^{1}H NMR ($CDCl_3$, 400 MHz): δ 7.54−7.49 (m, 4H); 7.47−7.41 (m, 8H); 6.77 (dt, 2H, J = 7.2 Hz, J = 1.6 Hz); 6.65 (dt, 2H, J = 7.2 Hz, J = 1.6 Hz); 6.52 (dd, 2H, J = 7.2 Hz, J = 1.6 Hz); 5.23 (s, 1H); 3.90 (s, 6H); 2.21 (s, 6H); 1.69 (s, 6H). TOF MS ES: MH^+ m/z: calc. 786.2546 found: 786.2534 Anal. Calcd. for $C_{39}H_{37}IrN_4O_2.CH_2Cl_2$: C, 55.17; H, 4.51; N, 6.43. Found: C, 54.97; H, 4.43; N, 6.38.

5a: The dimeric iridium(III) complex **5** (75 mg; 0.038 mM) was dissolved in 80 mL of dichloromethane under argon. To this solution was added acetylacetone (20 mg, 0.20 mM) and tetrabutylammonium hydroxide (162 mg, 0.21 mM). The reaction mixture was refluxed under argon overnight. After being cooled to RT, the solvents were evaporated to dryness. The crude obtained was purified with a short column chromatography (SiO_2, CH_2Cl_2). The major yellow band was collected to afford **5a** as yellow solid (47 mg, 48%). ^{1}H NMR ($CDCl_3$, 400 MHz): δ 7.47−7.38 (m, 6H); 7.38−7.32 (m, 4H); 7.28−7.15 (m, 10H); 6.63 (m, 4H); 6.41 (m, 2H); 6.18 (d, 2H, J = 2.7 Hz); 5.29 (s, 1H); 2.33 (s, 6H); 1.80 (s, 6H). TOF MS ES: MH^+ m/z: calc. 910.2859 found: 910.2839 Anal. Calcd. for $C_{49}H_{41}IrN_4O_2$: C, 64.67; H, 4.54; N, 6.16. Found: C, 64.57; H, 4.42; N, 6.09.

6a: The dimeric iridium(III) complex **6** (110 mg; 0.079 mM) was dissolved in 150 mL of dichloromethane under argon. To this solution was added acetylacetone (60 mg, 0.60 mM) and tetrabutylammonium hydroxide (330 mg, 0.428 mM). The reaction mixture was refluxed under argon overnight. After being cooled to RT, the solvents were evaporated to dryness. The crude obtained was purified with a short column chromatography (SiO_2, CH_2Cl_2). The major yellow band was collected to afford **6a** as yellow solid (79 mg, 65%). ^{1}H NMR ($CDCl_3$, 400 MHz): δ 7.55−7.42 (m, 12H); 7.09 (s, 2H); 6.78 (dt, 2H, J = 7.2 Hz, J = 1.6 Hz); 6.68 (dt, 2H, J = 7.2 Hz, J = 1.6 Hz); 6.54 (dd, 2H, J = 7.2 Hz, J = 1.6 Hz); 5.30 (s, 1H); 4.10 (s, 6H); 1.78 (s, 6H). TOF MS ES: MH^+ m/z: calc. 758.2233 found: 758.2199 Anal. Calcd. for $C_{37}H_{33}IrN_4O_2$: C, 58.64; H, 4.39; N, 7.39. Found: C, 58.45; H, 4.30; N, 7.28.

Scheme 2. Synthetic Strategy for the Ligands

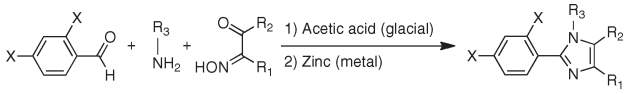

Results and Discussion

The various ligands have been synthesized following a one-pot condensation strategy to form the imidazole ring.[51] Instead of the more commonly utilized combination of diketone and ammonium acetate, the present syntheses are based on the use of a dione monoxime as starting material (Scheme 2).

This approach is particularly useful when a nonsymmetric substitution pattern is needed with R_1 different from R_2 (Chart 1). Indeed, in this case no isomer is found in the crude product, which makes the purification process much easier. After condensation, the imidazole oxide intermediate is not isolated but directly reduced using metallic zinc. Zinc has been used as granules or 10 μm powder. In both cases, zinc has been used directly as such or activated with hydrochloric acid before use. Unsurprisingly, it has been found that the most effective form of zinc to achieve the reduction is the activated 10 μm powder. In this case, the yields of reaction are much higher than with nonactivated granules. The preparation of the iridium complexes follows the usual two-step strategy. First, 2.5 equiv of ligand are refluxed overnight with $IrCl_3 \cdot xH_2O$ in a mixture of 2-ethoxyethanol and water to afford the chloro-bridged iridium dimer complex.[52] This dimer is then reacted with an excess of ancillary ligand and tetrabutylammonium hydroxide as a base in dichloromethane as a low boiling solvent to give the desired mononuclear iridium complex. Purification was achieved either by column chromatography on silica gel, Sephadex LH-20, recrystallization, or a combination of these techniques. It should be noted that yields of synthesis for all complexes are low to very low, particularly compared to yields usually obtained during synthesis of complexes based on a phenyl-pyridine ligand. This might be due to the increased basicity of imidazole compared to pyridine making the purification over silica gel column unsuitable. In general, better yields and higher purity can be obtained when the crude reaction is directly filtered on a very short plug of silica gel, eluting with dichloromethane containing 0−1% of methanol if needed (see **4a**, **5a**, and **6a**). The main yellow band is collected and the solvent is removed under reduced pressure. The crude product is dissolved in the minimum of dichloromethane and poured into a large amount of hexane to isolate the complex.

These syntheses led to two series of complexes. One consists of acetylacetone (acac) as the ancillary ligand. The purpose is to study the influence on the photo- and electrochemical properties of the complexes of the positioning of the methyl and phenyl groups on the imidazole ring. The second series consists of complexes with various ancillary ligands.

The absorption spectra of the complexes in dichloromethane solution are shown in Figure 1 for the acac-based series and in Figure 2 for the nonacac-based series. It should be noted that complexes are apparently poorly stable when exposed to light and oxygen both in solution and in the solid state as the color turns brownish within a couple of days.

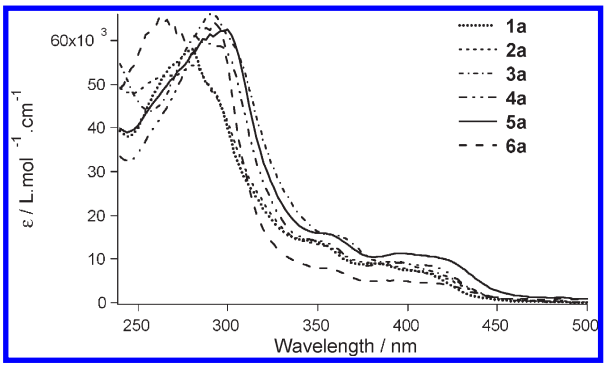

Figure 1. Absorption spectra of acetylacetone-based complexes in CH_2Cl_2 solution at room temperature.

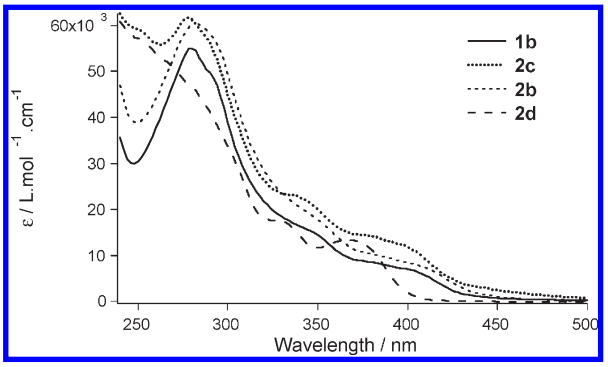

Figure 2. Absorption spectra of nonacetylacetone-based complexes in CH_2Cl_2 solution at room temperature.

All complexes display strong absorption bands in the UV region with a molar extinction coefficient between 50 000 and 60 000 L mol^{-1} cm^{-1}. Those bands are assigned to $^1\pi-\pi^*$ transitions on the imidazole ligand. **2d** is an exception as no clear band is observed but a broad shoulder is seen at wavelength lower than 320 nm. Compared to acac, the ancillary ligand (diphenylphosphino)ethanoic acid P is expected to stabilize the highest occupied molecular orbitals (HOMO) of the complex due to the *d*-orbital contribution of the phosphorus atom, much more than the LUMO orbital. This should ultimately increase the HOMO−LUMO energy gap and a blue shift of the emission should be observed (see below).[53,54] It appears that complexes with additional phenyl rings on the imidazole show similar absorption intensity in the UV part of the spectra. This is attributed to the presence of methyl groups in proximity to the phenyl substituents. The steric hindrance forces the phenyls to be orthogonal to the imidazole ring (see X-ray crystal structures below), which effectively decreases the electronic coupling between the two chromophores.[55] The extinction coefficients of the multichromophoric materials are then considered as additive.[56,57] The extinction coefficient of benzene is about

(51) Lousame, M.; Fernandez, A.; Lopez-Torres, M.; Vazquez-Garcia, D.; Vila, J. M.; Suarez, A.; Ortigueira, J. M.; Fernandez, J. J. *Eur. J. Inorg. Chem.* **2000**, 2055.

(52) Nonoyama, M. *Bull. Chem. Soc. Jpn.* **1974**, *47*, 767.

(53) Chiu, Y.-C.; Chi, Y.; Hung, J.-Y.; Cheng, Y.-M.; Yu, Y.-C.; Chung, M.-W.; Lee, G.-H.; Chou, P.-T.; Chen, C.-C.; Wu, C.-C.; Hsieh, H.-Y. *ACS Appl. Mater. Inter* **2009**, *1*, 433.

(54) Chiu, Y.-C.; Hung, J.-Y.; Chi, Y.; Chen, C.-C.; Chang, C.-H.; Wu, C.-C.; Cheng, Y.-M.; Yu, Y.-C.; Lee, G.-H.; Chou, P.-T. *Adv. Mater.* **2009**, *21*, 2221.

(55) Beaven, G. H.; Johnson, E. A. *Spectrochim. Acta* **1959**, *14*, 67.

(56) Flamigni, F.; Baranoff, E.; Collin, J.-P.; Sauvage, J.-P. *Chem.—Eur. J.* **2006**, *12*, 6592.

Table 1. Photophysical[a] and Electrochemical Properties of Complexes[b]

	λ_{abs}/nm	λ_{em}/nm	τ/ns	Φ_p	$E_{1/2red}$[c]	$E_{1/2ox}$[c]
1a	280, 350, 386, 412	487, 522	145	0.047	-3.29_i	0.12
1b	278, 346, 404	485, 520	517	0.11	−2.87	0.20
2a	282, 350, 416	510sh, 540	740	0.43	-2.59_i	0.19
2b	280, 352, 406	539	1635	0.22	−2.84	0.26
2c	278, 342, 400	591	92	0.038	−2.55	0.35
2d	330, 366	538	24	0.002	-2.95_i	0.28
3a	290, 364, 398, 418	570	1057	0.25	-2.72_i	0.52
4a	286, 354, 396, 416	547	1108	0.40	−2.48	0.19
5a	300, 356, 396, 422	517sh, 551	1890	0.95	−2.94	0.25
6a	262, 356, 390, 422	557	662	0.32	−2.53	0.19
N966[d]	260, 308, 348, 440	570	29	0.015	−3.30	0.17

[a] In degassed dichloromethane solution at room temperature. [b] Potentials are given to ferrocene as internal reference. [c] Conditions: working electrode glassy carbon, counter electrode sputtered Pt; reference electrode Pt wire. DMF, NBu_4PF_6 0.1 M. i: irreversible, wave peak given. [d] From ref 36; redox potential measured in DMSO.

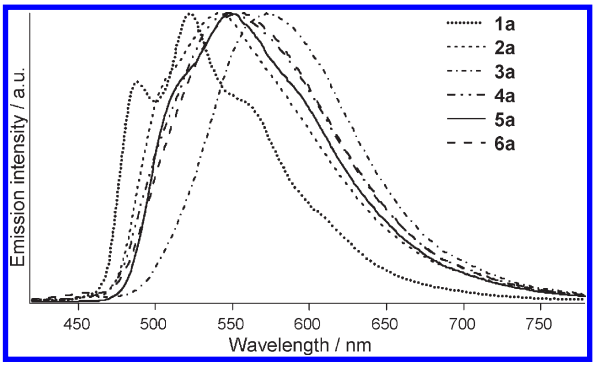

Figure 3. Emission spectra of acetylacetone-based complexes in CH_2Cl_2 solution at room temperature.

200 L mol^{-1} cm^{-1} at 254 nm,[58,59] which is negligible compared to the ε value (~60 000 L mol^{-1} cm^{-1}) of **1a**. In the near-UV and visible range, weaker absorption bands with molar extinction coefficients around 10 000 L mol^{-1} cm^{-1} are assigned to metal-to-ligand charge transfer (MLCT) transitions. Once again **2d** stands out as an exception with the lowest energy absorption band being at 366 nm, with almost no tail extending in the visible part of the spectrum, which makes the complex colorless.

When the complexes in dichloromethane solution are excited at room temperature in the MLCT band (400 nm), they emit from bluish-green to orange (Table 1). The emission spectra of acac-based complexes are shown in Figure 3 and the emission spectra for the complexes having different ancillary ligands are shown in Figure 4. Using only methyl and phenyl groups and by modifying simply the substitution pattern on the imidazole ring, the emission maxima can be tuned from 520 to 591 nm. In the case of **1a**, which has the imidazole ring fully substituted with methyl groups, the emission maximum is observed at 522 nm with a higher energy band of lower intensity at 488 nm. Replacing the methyl group on the nitrogen by a phenyl (i.e., complex **2a**) shifts the emission maximum to 540 nm. In addition, the shape of the spectrum becomes less structured, suggesting an increased MLCT character. In **5a**, a second methyl group is

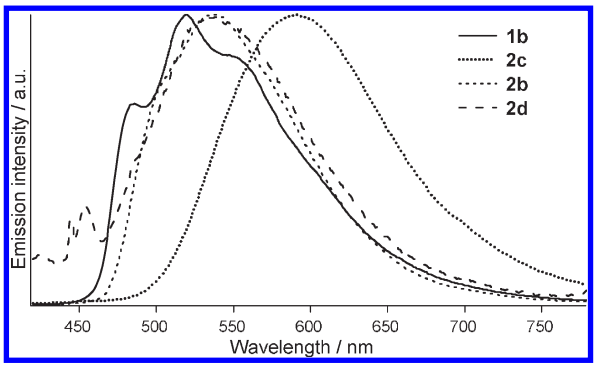

Figure 4. Emission spectra of non-acetylacetone-based complexes in CH_2Cl_2 solution at room temperature.

replaced with the less electron donating phenyl group, which resulted in an additional red shift of the emission maximum of 11 nm. Finally, in **6a** where the last methyl group is replaced by hydrogen, the emission is further red-shifted by 6 nm. In phenyl-pyridine based iridium complexes, it is known that the addition of donor groups on the pyridine ring leads to a blue shift of the emission mainly through destabilization of the LUMO energy level of the complex.[13−18] From our results, the same trend is observed using an imidazole ring instead of pyridine. Therefore, as a first approximation, the trend in emission maxima can be rationalized by saying that the imidazole ring has a significant LUMO character. Therefore, a decrease of the number of donor substituents on the imidazole ring stabilizes the LUMO more than the HOMO, leading to a reduced HOMO−LUMO gap, that is, a red shift of emission.

It is particularly interesting to compare **2a** and **4a** as they are isomers relative to the positions of the methyl and phenyl groups on the R_2 and R_3 substituents, with R_2 = Me and R_3 = Ph for **2a** and R_2 = Ph and R_3 = Me for **4a**. This exchange between the methyl and phenyl positions induces a 7 nm red shift of the emission. This shows that the donor influence of the methyl group is stronger when attached to the nitrogen atom. Therefore, it can be deduced that the nitrogen atom is likely to be more directly involved in the LUMO orbital than in the HOMO orbital.

Complex **3a** is worth discussing more in detail as it exhibits counterintuitive emission maximum. The complex **3a** is the same as **1a** with two chloro-substituents in 2 and 4 positions of the orthometalated phenyl ring. Chlorine acts as an acceptor group based on its Hammett parameter,[60] and therefore a blue shift of the emission maximum could have been expected by analogy with widely used fluoro substituents. Indeed, it is generally accepted that acceptor substituents on the cyclometalated phenyl ring tend to stabilize the HOMO of the complex more than they stabilize the LUMO of the complex. It is well established in the case of ppy-based complexes. This is because usually the HOMO of the complex is mostly localized on the cyclometalated phenyl ring with a large contribution of the central metal atom.[61] Surprisingly, the chloro substitution in **3a** induces an emission maximum red shift of more than 50 nm when compared to **1a**.

As the emission spectra of **1a** and **3a** show very different shapes while the onsets of emission in dichloromethane may appear similar, a simple explanation could be emission

(57) Flamigni, F.; Ventura, B.; Baranoff, E.; Collin, J.-P.; Sauvage, J.-P. *Eur. J. Inorg. Chem.* **2007**, 5189.
(58) Du, H.; Fuh, R. A.; Li, J.; Corkan, A.; Lindsey, J. S. *Photochem. Photobiol.* **1998**, *68*, 141.
(59) Inagaki, T. *J. Chem. Phys.* **1972**, *57*, 2526 and references therein.
(60) Hansch, C.; Leo, A.; Taft, R. W. *Chem. Rev.* **1991**, *91*, 165.
(61) Hay, P. J. *J. Phys. Chem. A* **2002**, *106*, 1634.

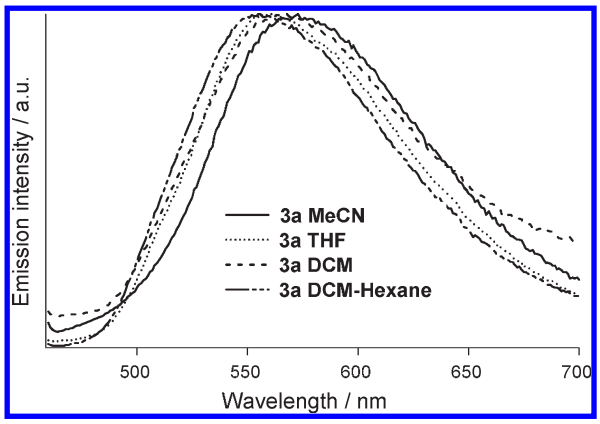

Figure 5. Emission spectra of **3a** in various solvents. DCM−hexane is a 1:4 mixture of dichloromethane and hexane, respectively.

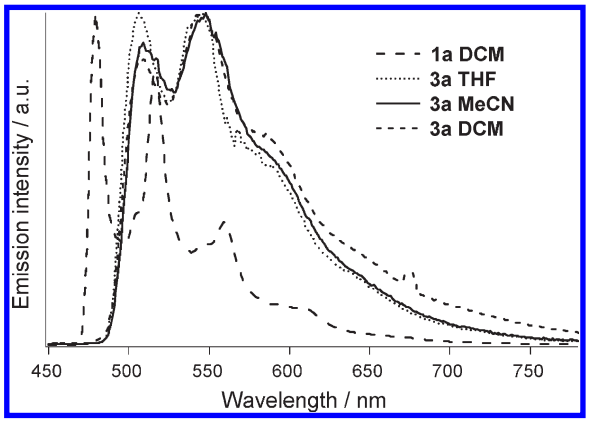

Figure 6. Emission spectra at 77 K of **1a** in dichloromethane and **3a** in dichloromethane, acetonitrile, and tetrahydrofuran.

solvatochromism due to an increase of the MLCT character in **3a**. To verify this hypothesis, we measured the emission of **3a** in various solvents with different polarities (Figure 5). A red shift of the emission maximum is observed in more polar solvents as expected for an emission with significant MLCT character. However, the emission shape does not change much and the shift of emission maximum is limited to 20 nm from DCM−hexane to acetonitrile, which is much smaller than the 50 nm red-shift observed from **1a** to **3a**. Therefore, a solvent effect is unlikely to be the cause for the observed red shift in **3a** compared to **1a**. To gain further insight into the emission properties of **1a** and **3a**, we recorded the emission spectra at 77 K (Figure 6). The spectra of **3a** show more structure with a vibronic progression and peaks separated by about 1450 cm^{-1}. Compared to the emission maximum at room temperature, the emission maximum at 77 K is significantly blue-shifted to about 507 nm for all solvents. On the other hand, the solvatochromic shift is reduced to only 5 nm.[62] Again, this shows that the influence of the solvent is very unlikely to be the cause of the red-shifted emission of **3a** compared to **1a**. The spectrum of **1a** in dichloromethane at 77 K is highly structured with bands at 479, 516, 560, 610, and about 670 nm. All peaks in this main vibronic series are separated as well by about 1450 cm^{-1}. Few additional shoulders of lower intensity are observed in the spectrum. They are attributed to internal ligand modes other than vibrations of carbon−carbon double bond.[63] It should be noted that at low temperature the separation between the emission maxima of **1a** and **3a** is 1100 cm^{-1}, while it is 3000 cm^{-1} at room temperature. This suggests that significant stabilization occurs in the excited state of **3a** at room temperature leading to a low energy triplet excited state. This is further supported by theoretical calculations performed on **1a** and **3a** (see below).

In the second series, the use of different ancillary ligands allows further tuning of the band shape and emission maximum. In the case of **1b**, the emission maximum is nonsignificantly blue-shifted compared to **1a**. The main change is a broadening of the emission spectrum by 640 cm^{-1}. The use of picolinic acid as ancillary ligand in **2c** leads to unstructured orange emission centered at 591 nm. As complexes **2a**, **2b**, and **2d** have very similar emission maxima, the result of **2c** can be explained by emission from the ancillary ligand Pic, somehow related to an interligand energy transfer.[64−66] Indeed, the energy level of the LUMO of Pic is much lower than the dimethylamino substituted pic, NPic, and that of acac and P. In the case of **2d**, the similar emission maximum to **2a** came as a surprise. As expected, the HOMO is indeed stabilized as shown by the oxidation potentials (see below). This means that the LUMO orbital is affected by the ancillary ligand pointing to a significant LUMO character on the phenyl. Combined with the above-discussed substituent effect on the imidazole ring, this suggests that the LUMO is more delocalized on the entire ligand in contrast to the phenyl-pyridine case.

Photoluminescence quantum yields Φ_p range from very poor for **2d** to very high for **5a**. It can be noted that the quantum yields tend to increase with the number of phenyl substituents on the imidazole. As the phenyls are orthogonal to the imidazole, effectively cutting off the electronic communication between the two groups, they are not expected to have a significant electronic impact on the quantum yields, except perhaps for stabilizing the LUMO. This could increase the energy gap with the deactivating MC state. However, in this case, **6a** could have shown a better quantum yield. Therefore, the phenyl rings could simply isolate the complex from the surrounding solvent, effectively decreasing the nonradiative deactivation through solvent vibrations. The low quantum yield of **2d** is likely due to the flexibility of P.[54] In **2c**, the low quantum yield is attributed to emission from Pic and not from the main ligand similar to what has been observed with ppy.[67] Radiative lifetimes τ_{rad} are in the microsecond range as expected for cyclometalated iridium(III) complexes. Different lifetimes are observed for the two positional isomers **2a** and **4a** and **2a** shows the shorter lifetime. This points toward differences in the emitting excited state. These differences obviously originate from the different positions of the phenyl and methyl groups on the imidazole.

Oxidation and reduction potentials of the complexes have been obtained by cyclic voltammetry in DMF. Oxidations

(62) The solvent mixture DCM−hexane gave emission spectrum with lot of defects, likely coming from low quality glass. Therefore, it is not reproduced in the figure. It is essentially the same as with other solvents.

(63) Rausch, A. F.; Homeier, H. H. H.; Yersin, H. *Top. Organomet. Chem.* **2010**, *29*, 193.
(64) You, Y.; Park, S. Y. *J. Am. Chem. Soc.* **2005**, *127*, 12439.
(65) You, Y.; Kim, K. S.; Ahn, T. K.; Kim, D.; Park, S. Y. *J. Phys. Chem. C* **2007**, *111*, 4052.
(66) You, Y.; Seo, J.; Kim, S. H.; Kim, K. S.; Ahn, T. K.; Kim, D.; Park, S. Y. *Inorg. Chem.* **2008**, *47*, 1476.
(67) Xu, M. L.; Zhou, R.; Wang, G. Y.; Xiao, Q.; Du, W. S.; Che, G. B. *Inorg. Chim. Acta* **2008**, *361*, 2407.

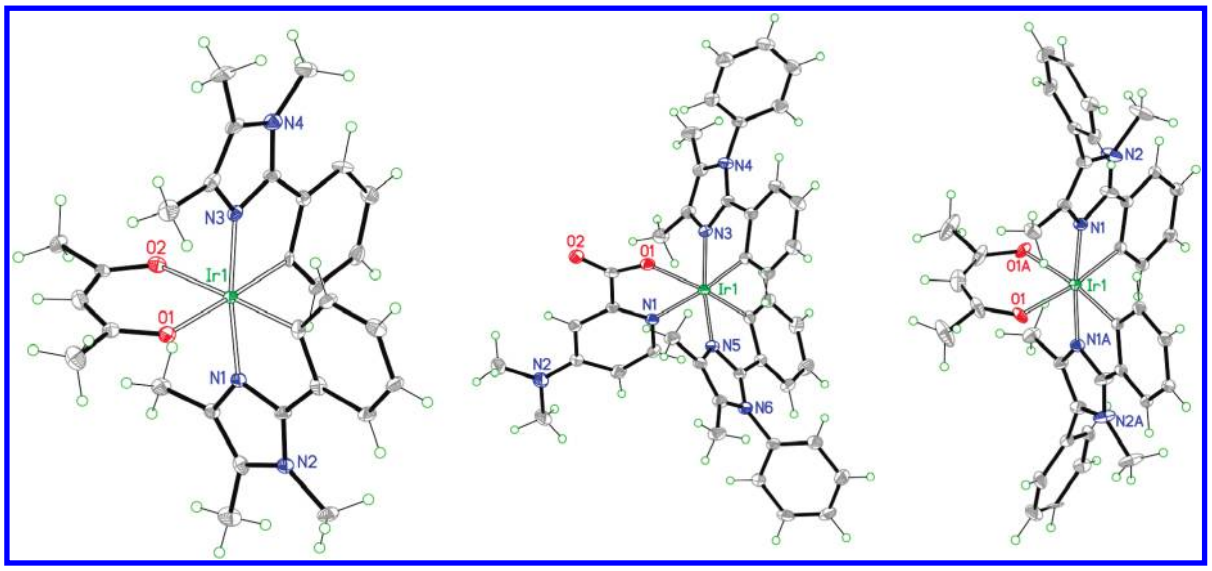

Figure 7. ORTEP drawings of **1a**, **2b**, and **4a**.

are reversible and their values are influenced by the substituents on the imidazole ring. Indeed, **1a**, **2a**, **4a**, and **5a** are respectively oxidized at 0.12, 0.19, 0.19, and 0.25 V vs ferrocene. In this case, the isomers **2a** and **4a** exhibit no measurable difference in oxidation potential. Replacing the methyl by phenyl groups increases the oxidation potential (i.e., the HOMO of the complex is stabilized). As the substituents on the imidazole ring can significantly influence the HOMO energy level, this suggests that the imidazole possesses significant HOMO character. The presence of chlorine in **3a** induces, as expected, a strong stabilization of the HOMO level resulting in an oxidation potential of 0.52 V vs ferrocene. The donor character of the dimethylamino group can be observed when **2b**, which has NPic as ancillary ligand, and **2c**, which has Pic as ancillary ligand, are compared. Indeed, the oxidation potential of **2b** is lower, indicating a destabilization of the HOMO energy by the donor group on the ancillary ligand.[68−71] The reduction potentials are much less conclusive for general trends as mostly irreversible waves are observed. The disparity of the remaining reversible reductions points to a variety of ground state LUMO localization. Besides **2c** where the LUMO of the complex can be reasonably anticipated to be mainly on the picolinate ancillary ligand, other complexes seem to be highly dependent on the substitution pattern of the imidazole ring. This is expected as the imidazole has a significant LUMO character. On the other hand, as the LUMO localized on the main and ancillary ligands are close in energy, precise assignment based solely on redox potentials is not a simple task.

Overall, one can conclude that, based on electrochemical results, the HOMO and LUMO energy levels of imidazole-based complexes lie at higher energy levels compared to related complexes based on phenyl-pyridine cyclometalated ligands. In addition, while the imidazole ring is mostly of LUMO character and the HOMO is mostly located on the phenyl and the iridium center (similar to phenyl-pyridine based complexes), these molecular orbitals are more delocalized over the entire main ligand compared to the case of phenyl-pyridine where they are fairly well localized. This is consistent with previous observations.[36]

The X-ray crystal structures of **1a**, **2b**, and **4a** are shown in Figure 7, and their crystallographic data are shown in Table 2. Single crystals were grown by slow diffusion of hexane in a dichloromethane solution of the complex. The geometry around the iridium center is a slightly distorted octahedron with the methyl group in the α position of the nitrogen coordinated to the iridium likely inducing most of the distortion as it is pointing into the ancillary ligand. As expected for these complexes prepared at low temperature, the two imidazole rings are coordinated in the trans configuration in contrast to the high temperature case.[72]

To provide insight into the structural, electronic, and optical properties of the investigated complexes, we performed DFT/TDDFT calculations on the selected compounds **1a** and **3a**, for which counterintuitive spectroscopic data have been obtained.

Geometry optimizations were performed on both the ground singlet and lowest triplet excited states of **1a** and **3a**, the latter corresponding to the lowest SCF triplet states. The calculated optimized structural parameters for the ground and excited states of the investigated complexes are reported in Table 3 and compared to the X-ray geometry of **1a**. The agreement between ground state calculated structural data and available experimental parameters is good, and minor differences in the metal coordination sphere are computed between the two complexes. We notice, however, that the steric hindrance exerted by the Cl-substituent in **3a**, leads to an out-of-plane displacement of the Cl atoms by ca. 10°; see the ∠ClCCC dihedral angle in Table 3 and Figure 8, while in **1a** the corresponding H atom essentially lies in the ligand plane. Moving to the excited state geometries, both

(68) De Angelis, F.; Fantacci, S.; Evans, N.; Klein, C.; Zakeeruddin, S. M.; Moser, J.-E.; Kalyanasundaram, K.; Bolink, H. J.; Grätzel, M.; Nazeeruddin, M. K. *Inorg. Chem.* **2007**, *46*, 5989.
(69) Bolink, H. J.; Coronado, E.; Santamaria, S. G.; Sessolo, M.; Evans, N.; Klein, C.; Baranoff, E.; Kalyanasundaram, K.; Graetzel, M.; Nazeeruddin, M. K. *Chem. Commun.* **2007**, 3276.
(70) Minaev, B.; Minaeva, V.; Agren, H. *J. Phys. Chem. A* **2009**, *113*, 726.
(71) Zhang, M.; Li, Z.-S.; Li, Y.; Liu, J.; Sun, J.-Z. *Int. J. Quantum Chem.* **2009**, *109*, 1167.
(72) Baranoff, E.; Suàrez, S.; Bugnon, P.; Barolo, C.; Buscaino, R.; Scopelliti, R.; Zuppiroli, L.; Graetzel, M.; Nazeeruddin, M. K. *Inorg. Chem.* **2008**, *47*, 6575.

Table 2. Crystallographic Data for **1a**, **2b**, and **4a**

	1a·1.7CH_2Cl_2	**2b**·2CH_2Cl_2	**4a**
empirical formula	$C_{30.7}H_{36.4}Cl_{3.4}IrN_4O_2$	$C_{44}H_{43}Cl_4IrN_6O_2$	$C_{39}H_{37}IrN_4O_2$
formula weight	806.17	1021.84	785.93
temperature, K	100(2)	100(2)	140(2)
wavelength (Å)	0.71073	0.71073	0.71073
crystal system	triclinic	triclinic	monoclinic
space group	$P\bar{1}$	$P\bar{1}$	$I2/a$
unit cell dimensions			
a (Å)	9.2362(17)	10.0882(16)	16.517(3)
b (Å)	13.6956(15)	11.9006(6)	10.650(2)
c (Å)	14.136(2)	19.0655(17)	19.517(4)
α (deg)	69.463(10)	76.990(8)	90
β (deg)	83.415(14)	84.823(9)	103.68(3)
γ (deg)	77.185(9)	67.972(9)	90
volume (Å^3)	1631.5(4)	2067.3(4)	3335.6(11)
Z	2	2	4
density, calcd (g/cm^3)	1.641	1.642	1.565
absorption coefficient (mm^{-1})	4.404	3.534	4.043
F(000)	799	1020	1568
crystal size (mm^3)	0.49 × 0.39 × 0.31	0.36 × 0.29 × 0.29	0.40 × 0.32 × 0.20
θ range for data collection (deg)	3.03−27.50	3.10−27.5	2.54−27.58
reflections collected	27355	38788	10194
independent reflections	7401 [R(int) = 0.0584]	9426 [R(int) = 0.0406]	3730 [R(int) = 0.0662]
refinement method	full-matrix least-squares on F^2	full-matrix least-squares on F^2	full-matrix least-squares on F^2
data/restraints/parameters	7401/54/407	9426/0/514	3730/168/260
goodness-of-fit on F^2	1.209	1.135	1.109
final R indices [$I > 2\sigma(I)$]	R_1 = 0.0473	R_1 = 0.0246	R_1 = 0.0602
	wR_2 = 0.1242	wR_2 = 0.0579	wR_2 = 0.1406
R indices (all data)	R_1 = 0.0565	R_1 = 0.0308	R_1 = 0.0633
	wR_2 = 0.1291	wR_2 = 0.0618	wR_2 = 0.1427

Table 3. Comparison between Calculated Geometrical Structures and Average of Available Experimental Data for **1a** and **3a** Complexes[a]

	1a			**3a**	
parameter	<exp>	S_0	T_1	S_0	T_1
Ir−N	2.057	2.049	2.044	2.039	2.037
Ir−C	2.007	2.003	1.998	1.995	1.979
Ir−O	2.156	2.172	2.159	2.162	2.170
C−C	1.402	1.442	1.418	1.458	1.420
∠N−Ir−N	172.1	171.8	172.2	173.1	173.6
∠O−Ir−O	88.3	88.4	87.7	88.4	86.6
∠N−Ir−C	79.8	79.8	80.5	79.0	80.2
∠N−Ir−O	98.4	97.8	97.2	99.5	99.1
∠CNCC	1.61	2.5	1.6	3.2	15.4
∠H(Cl)CCC	1.65	1.6	0.2	10.3	16.1

[a] ∠CNCC refers to the dihedral angle between the methyl-imidazole and the phenyl moieties of the cyclometalated ligand in **1a** and **3a**. ∠H(Cl)CCC refers to the dihedral angle between the H(Cl) of the phenyl moiety and the imidazole carbon in the cyclometalated ligand for **1a** (**3a**).

complexes exhibit similar structural variations compared to the ground state, except the dihedral angle characterizing the relative arrangement of the imidazole and phenyl moieties of the cyclometalated ligand (∠CNCC in Table 3). While this parameter is close to zero in the ground state of **1a** and **3a**, the ∠CNCC dihedral angle substantially increases in the triplet excited state of **3a** (3.2 vs 15.4°, in S_0 and T_1, respectively), while it remains essentially constant in **1a** (2.5 vs 1.6°). A similar behavior is observed also for the ∠ClCCC dihedral angle. Thus, a considerable distortion from planarity is calculated for the excited state of **3a**, which leads to an additional stabilization of the excited state for this complex; see below.

A molecular orbital energy diagram calculated for the singlet-optimized geometries for **1a** and **3a** is reported in Figure 9. A common feature of the investigated cyclometalated complexes is a HOMO made of the Ir d_{xy} orbital combined in an antibonding fashion with π orbitals of the cyclometalated ligand. The LUMOs are π^* combinations localized on the cyclometalated and acac ligands. A similar electronic structure is found for **1a** and **3a**, even though a sizable stabilization of both occupied and unoccupied molecular orbitals is predicted for the latter, with an associated slight reduction of the HOMO−LUMO gap; see Figure 9. Moreover, while in **1a** the acac-based orbital is the LUMO+1, in **3a** the same orbital is the LUMO+2. Our calculated electronic structure is fully consistent with electrochemical data obtained in the context of the present investigation for **1a** and **3a**. This shows a strong positive shift of both the oxidation and reduction potentials by 0.40 and 0.57 V, respectively, going from **1a** to **3a**. This is paralleled by a calculated positive HOMO and LUMO shift of 0.52 and 0.48 eV, respectively. It should be noted that the experimental value of the positive shift of the reduction potential going from **1a** to **3a** may not be quantitatively exact as both waves are irreversible. Moving from S_0 to T_1 optimized geometries,

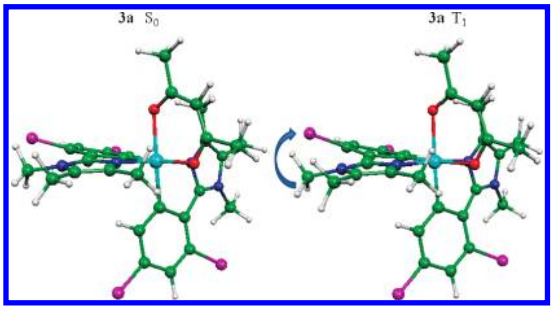

Figure 8. Optimized molecular structures of **3a** in its ground and excited state.

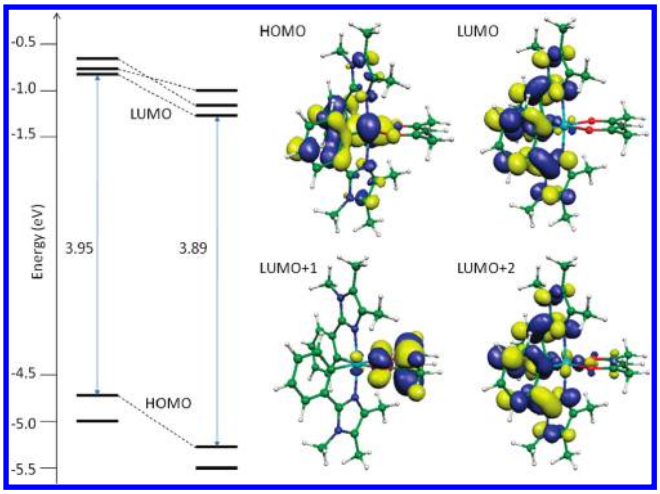

Figure 9. Molecular orbital energy diagram for **1a** and **3a** and isodensity plots of selected orbitals for **1a**.

Table 4. Calculated Lowest Excitation Energies (nm) at Both the Singlet and Triplet Geometries for **1a** and **3a**[a]

	1a		**3a**	
	S_0	T_1	S_0	T_1
$S_0 \rightarrow T_1$	446	485	460	528
$S_0 \rightarrow T_2$	440	476	457	519
$S_0 \rightarrow T_3$	438	456	426	429
$S_0 \rightarrow S_1$	393 (0.005)	413 (0.004)	397 (0.092)	430 (0.111)
$S_0 \rightarrow S_2$	387 (0.093)	412 (0.100)	380 (0.04)	409 (0.007)
$S_0 \rightarrow S_3$	379 (0.002)	400 (0.002)	367 (0.024)	386 (0.026)

[a] For singlet−singlet transitions oscillator strengths are also reported.

we observe a reduction of the HOMO−LUMO gap from 3.95 (3.89) to 3.74 (3.57) eV for **1a** (**3a**). The larger HOMO−LUMO gap reduction calculated for **3a** (0.21 vs 0.32 eV) is related to the excited state structural distortion discussed above. It is also interesting to notice that for the analogous **N966** complex we calculated three almost degenerate LUMOs of mixed character, distributed among the acac and cyclometalated ligands. In contrast, for **1a** the three orbitals are essentially fully localized on either ligand. The peculiar LUMOs mixing in **N966** was related to the broad and unstructured emission exhibited by that complex, as opposed to the narrower and the well-resolved emission found for **1a**; see Figure 3.

We now move to the descriptions of the excited states of **1a** and **3a**, which are summarized in Table 4. In line with the electronic structure picture discussed above, the lowest transition energies in **3a** are red-shifted compared to those calculated for **1a**. This behavior is particularly evident if one considers the excited states related to the emission process, that is, the $S_0 \rightarrow T_1$ transitions calculated at the T_1 optimized geometries; in this case, a red-shift from 485 to 528 nm is calculated going from **1a** to **3a**, which is perfectly paralleled by the HOMO−LUMO gap decrease due to the excited state structural distortion.

A comparison between calculated transition energies and the experimental emission spectra at room temperature is not straightforward, since **1a** and **3a** have rather different emission profiles, with **1a** (**3a**) showing a structured (unstructured) emission. We recall indeed that for a given electronic transition, the emission profile is determined by Franck−Condon

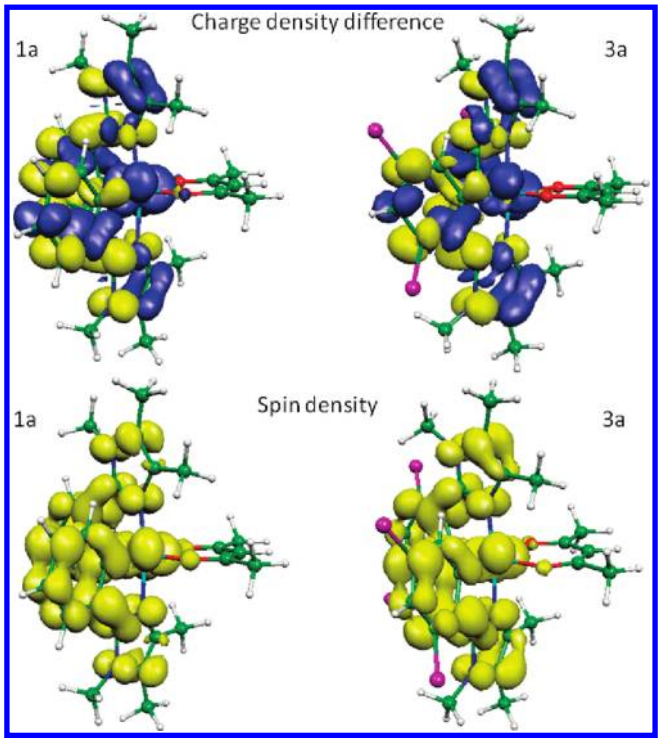

Figure 10. Upper panel: charge density difference between the lowest excited triplet TDDFT state and the ground state (contour value 0.001). Lower panel: spin density of the unrestricted triplet state (contour value 0.002).

factors related to the overlap between vibrational wave functions for the ground and excited states, which we are not including in our description.

For **1a** a clear vibronic progression can be distinguished with features at 487 and 522 nm, and an associated peak separation of ca. 1380 cm^{-1}, typical of the aromatic C−C stretching of the cyclometalated ligands. Our calculated transition at 485 nm nicely compares with the blue end of the emission spectrum. For **3a** a broad emission is found, peaking at 570 nm. Converting into energy units and adding 1380 cm^{-1} to the emission maximum wavenumber, we can estimate a transition at ca. 530 nm, which nicely compares to our calculated data of 528 nm. As anticipated from experimental data, it should be noted that phenyl-imidazole and phenyl-pyridine based complexes differ rather fundamentally in HOMO and LUMO localization. While in the case of phenyl-pyridine, it is well accepted that the HOMO is mostly localized on the coordinated phenyl and the LUMO mostly localized on the pyridine ring, in the case of phenyl-imidazole both HOMO and LUMO are mostly delocalized over the entire cyclometalated ligand. This could explain why the LUMO energy level of **3a** is significantly affected by the distortion induced by the chloride substituents.

It is finally interesting to provide a visual representation of the charge flow associated to the emission process. The most rigorous way to approach this issue is that of plotting the charge density difference between the ground and excited state, as derived by a ground state DFT and an excited state TDDFT calculation, respectively. Alternatively, one might look at the spin density distribution in the lowest triplet state, as obtained by an unrestricted DFT calculation, as representative of the excited state electron distribution. Both types of plots are reported in Figure 10.

As it can be noticed, both graphical representations provide a similar picture of the excited states for **1a** and **3a**, essentially related to charge reorganization involving the metal and the cyclometalated ligand, as might be expected from the nature of the HOMO and LUMO.

Conclusion

Two series of heteroleptic complexes based on a phenylimidazole as the main ligand have been synthesized and characterized electrochemically and photophysically. We have shown that emission wavelength can be tuned by applying known strategies used with complexes based on phenyl pyridine as main ligand. Differences are however observed as the HOMO and LUMO orbitals of imidazole based complexes are lying at higher energy and are less localized on the cyclometalated ring and the imidazole ring, respectively, than with phenyl-pyridine ligands. Interestingly, by using chloro substituents as strong acceptor groups a red shift of emission is observed instead of the expected blue-shift. This appears to be due to a significant geometrical and electronic relaxation accompanying the formation of the emitting excited state in this complex.

We are now investigating this family of complexes more in detail in order to fully understand the parameters controlling the broadness of the emission spectrum. We hope then to be able to improve the photophysical properties of **N966** for single emitting center WOLED with improved performances.

Acknowledgment. We acknowledge financial support for this work by Solvay S.A., DCTRP New Business Development. Z.X. also acknowledges financial support from the National Natural Science Foundation of China (No. 20501011).

Supporting Information Available: Crystallographic information files. This material is available free of charge via the Internet at http://pubs.acs.org.